Comparative analysis of marine traffic flow in classical models

Huang, Yamin; Yip, Tsz Leung; Wen, Yuanqiao

DOI
10.1016/j.oceaneng.2019.106195

Publication date
2019

Document Version
Final published version

Published in
Ocean Engineering

Ocean Engineering 187 (2019) 106195

Contents lists available at ScienceDirect

Ocean Engineering

journal homepage: www.elsevier.com/locate/oceaneng

Comparative analysis of marine traffic flow in classical models

Yamin Huang [a,b,c], Tsz Leung Yip [d,*], Yuanqiao Wen [a,b]

[a] Intelligent Transport Systems Research Center (ITSC), Wuhan University of Technology, Wuhan, 430063, China
[b] National Engineering Research Center for Water Transport Safety(WTSC), Wuhan, China
[c] Safety and Security Science Group, Faculty of Technology, Policy and Management, Delft University of Technology, Delft, the Netherlands
[d] Department of Logistics and Maritime Studies, The Hong Kong Polytechnic University, Hong Kong

ARTICLE INFO

Keywords:
Ship traffic
Fundamental diagram
AIS data
Empirical tests
Shanghai port

ABSTRACT

Traffic flow theory has been applied to the study of marine traffic flow and underpins the phenomena being studied. This paper is intended to demonstrate the uses of classical fundamental diagrams, which are developed previously on the basis of highway traffic, by conducting empirical tests on marine traffic data. Marine traffic data are extracted from the Automatic Identification System (AIS) from Shanghai port in 2010 and 2018. Interpolation methods are used to estimate the three primary variables of fundamental diagrams, namely, flow rate, traffic density, and local speed. The relationships among these three variables are discussed and marine traffic data are further compared and contrasted with classical traffic flow models. The importance of the finding is to create consistency, predictability and uniformity of uses of fundamental diagrams on marine traffic flow.

1. Introduction

The traffic flow theory has been recently used to underpin the phenomena of marine traffic flow. Wen et al. (2015) extended the concept of traffic flow complexity to marine traffic flow in terms of traffic density factor and traffic conflict factor. They argued the spatial distributions of traffic flow complexity and collision risk are highly correlated. Kang, Meng and Liu (2018) predicted the capacity of a waterway system by adopting the classical fundamental diagram of traffic flow. They used weighted and non-weighted least squared approaches to estimate the speed-density relationship of marine traffic along the Singapore Strait. They showed that the foundation of marine traffic flow theory is still highly deficient. Different from Kang et al. (2018), we are motivated to examine any difference(s) between marine traffic flow and classical traffic flow models.

The traffic flow model is the fundamental tool in traffic flow theory for describing, understanding, and predicting traffic flow. In maritime research, the microscopic models (individual ships) are popular, but the macroscopic flow model (a group of ships) has only recently emerged in the maritime literature (Jensen et al., 2013). Yip (2013) discussed a mathematical maritime flow model based on classical flow models. He proposed an extension of the one-dimensional Payne model to a two-dimensional marine traffic flow model, thereby introducing a new way of characterising maritime traffic flow.

In the marine domain, the automatic identification system (AIS) collects a vast amount of near-real-time traffic data. These data record ships' behaviour at different moments. According to the IMO's (International Maritime Organization's) regulation in SOLAS (the International Convention for the Safety of Life at Sea, 2000), AIS equipment is mandatory for vessels with gross cargo tonnages of 300 tons or more for international voyages, for vessels with gross cargo tonnages of 500 tons or more for non-international waterways, and for all passenger vessels whether in international or non-international waters. The requirement became effective for ships on 31 December 2004. Many researchers apply AIS to their research and studies.

However, although many kinds of traffic flow model have been used to describe maritime traffic flow, few of them have focused on the fundamental diagrams. The characteristics of the real-world traffic fundamental relationship in maritime traffic, and whether the maritime traffic fundamental diagram is similar to that of highway traffic flow, remain unclear. These issues are investigated in the remainder of this paper. Section 2 briefly summarises the traffic flow theory with respect to marine traffic. Section 3 presents an account of the methodology and explains the procedures of sampling used. Section 4 examines real-world traffic data sources and data pre-processing. Section 5 contains the results of empirical testing. Section 6 discusses the results. Section 7 concludes the study.

* Corresponding author.
E-mail addresses: y.m.huang@outlook.com (Y. Huang), t.l.yip@polyu.edu.hk (T.L. Yip), wenyqwhut@foxmail.com (Y. Wen).

https://doi.org/10.1016/j.oceaneng.2019.106195
Received 7 November 2018; Received in revised form 28 May 2019; Accepted 6 July 2019
Available online 5 August 2019

2. Literature review

2.1. Brief review of traffic flow theory

The initial research into the traffic flow model was conducted during the early twentieth century by Greenshields (1934), who studied the relationship between distance and velocity, known as the fundamental relationship (or fundamental diagram). After that, many types of traffic flow model have been developed to describe traffic flow phenomena. Generally, these investigations are categorised into microscopic models, mesoscopic models, and macroscopic models (van Wageningen-Kessels et al., 2014), the characteristics of which are described as follows.

2.1.1. Microscopic models

Microscopic models distinguish and trace the individual behaviour of each car, including actions such as car-following and lane-changing. Microscopic models include a leading vehicle and following vehicles, and each following vehicle will adjust its behaviour according to that of the leading vehicle. Currently, car-following models can be divided into four subtypes: safe-distance models (Gipps, 1981), stimulus-response models (Bando et al., 1995), action-point models (Wiedemann, 1974), and cellular-automata models (Nagel and Schreckenberg, 1992).

As a microscopic model can characterise the simple cooperation between vehicles, it is an accepted model type in the marine traffic field. In particular, maritime car-following models have been widely used in China to calculate the capacity of waterways and to simulate traffic. Zhu and Zhang (2009) used a ship-following model to calculate the transit capacity of an inland waterway; subsequently, He et al. (2012) improved the ship-following model and made it more suitable for marine traffic simulation. Feng (2013) used a different method, a cellar automata marine traffic flow model, which can also simulate traffic flow and calculate the transit capacity of waterways.

2.1.2. Mesoscopic models

Mesoscopic models describe the aggregate features of vehicle behaviour, such as the probability distribution of speed and density. Compared with micro- and macroscopic traffic models, the mesoscopic traffic model is the most recently developed type of model, and contains three main subtypes: headway distribution models (Buckley, 1968), cluster models (Mahnke and Kuhne, 2007), and gas-kinetic models (Prigogine, 1961). The gas-kinetic model is the most commonly used subtype in road traffic studies.

In the maritime traffic field, few models of the gas-kinetic subtype have been developed. However, some characteristics, such as arrival distribution, headway distribution, speed distribution, and density distribution, have become the main parameters to describe, predict, and simulate maritime traffic flow. Hou et al. (2014) used vessel speed, arrival time, and density, amongst other parameters, to describe traffic flow in the middle reach of the Yangtze River (including around the cities of Hefei, Wuhan, Nanchang, and Changsha). Other researchers have also used these parameters to predict traffic flow. Jagerman and Altiok (2003) analysed the arrival distribution of ships in sea ports to approximate both the asymptotic probabilities of the number of vessels and the waiting time probabilities. These parameters (i.e., vessel speed and arrival time) are the essential inputs to all types of traffic simulation models (Köse et al., 2003).

2.1.3. Macroscopic models

In macroscopic traffic models, traffic is regarded as a continuum flow. Such models ignore individual behaviour and focus on aggregated variables such as average density and velocity. The most basic macroscopic models were developed by Lighthill and Whitham (1955a,b) and Richards (1956), referred to as the LWR (Lighthill-Whitham-Richards) model. Subsequently, higher-order models, including cell transmission (CTM) (Daganzo, 1994) and multi-class (MC) LWR models, have been developed as improvements on the LWR model (Payne, 1971) (van Wageningen-Kessels et al., 2014).

Micro-, meso-, and macro-scopic models all have the same basis, which is the fundamental relationship between density, velocity, and flow rate. These models are dedicated to reproducing the key phenomena in real-world road traffic, such as capacity drop, hysteresis, and scattered fundamental diagrams (van Wageningen-Kessels et al., 2014). In other words, the fundamental diagram is the basis of traffic flow theory.

2.2. Traffic flow studies in maritime studies

Recently, with the spread of AIS equipment, more and more ship data become available for ship traffic flow analysis and have attracted numerous researchers working on ship traffic analysis. As Yip (2013) showed, the traffic flow model might benefit better safety management of ship traffic. In various studies, one popular type of traffic flow analysis dominates and aims at describing the statistical features of the ship traffic. In some other studies, researchers set a number of observation lines and calculating the number of the ships crossing these observation lines in different locations (Kasyk and Kijewska, 2013; Xiao et al., 2015). Then, the distributions of ship positions and ship speeds are obtained (Hou et al., 2014; Kasyk and Kijewska, 2013). Instead of analysing the traffic flow on the observation lines, other studies directly analyse the ship trajectories in a certain water area and identify the patterns of trajectory in the area on the basis of AIS data. For instance, Zhou et al. (2019) developed a naive Bayesian classifier for identifying ship's patterns in the port of Rotterdam; Chen et al. (2018) used the AIS data to classify vessel motion patterns in the Yangtze River. These statistical analyses are helpful for simulating traffic flow in the observed areas (Merrick et al., 2005; Xu et al., 2013) and conducting risk analysis in the observed waterways (Li et al., 2012).

Although the statistical analysis of ship traffic flow is useful to show the time-invariant feature of the traffic flow, the dynamics of traffic flow is neglected. In fact, the ship traffic flow also has time-varying features (e.g. density, average speed, flow), all of which are crucial for real-time traffic management. For instance, the vessel traffic control monitors the traffic flow so as to avoid a traffic congestion. More real-time traffic management in road traffic might refer to Qian (2009). In the maritime domain, there is a lack of tools to describe the dynamics of ship traffic flow for real-time traffic management.

The development of traffic flow analysis in road traffic has inspired a group of researchers in the maritime domain. Hongxiang et al. (2015) and Qi, Zheng, and Gang (2017a) simulated the ship traffic flow in a waterway by a famous cellular automaton model which is a widely used traffic flow model in road traffic. Later on, Qi, Zheng, and Gang (2017b) incorporated the influence of weather on ships' speed in a simulator. These studies showed the potential of using the traffic flow theory in ship traffic management. These studies, in fact, contain an assumption that the traffic law developed from the road traffic is readily applicable to ship traffic flow. However, this assumption has not been carefully tested in the maritime domain. That motivates this study to test the fitness of classical traffic flow models in the ship traffic flow. Kang, Meng and Liu (2018) conducted empirical tests of ship traffic flow in Singapore and showed that the relationship between density and speed of ship traffic is similar to the highway traffic models to some extent. The coefficient of overall fitness (R-squired statistics) ranges roughly from 0.4 to 0.9. However, they did not report other fundamental relationships.

3. Methodology

3.1. Definition of variables

To study the fundamental relation, the variables of traffic flow need to be first defined. Greenshields (1934) employed distance between vehicles and velocity as the fundamental parameters. Since

Greenshields' work, the main parameters for traffic flow have become: density (***k***), the average number of vehicles per unit length of road (*veh* /*m*); velocity (***u***), the average vehicle speed per unit length of road (*m* /*s*); and intensity (***q***), the average number of vehicles per unit time (*veh* /*s*).

In the maritime research field, a different measurement system exists, with the three variables above being defined as follows:

Density (***k***), the average number of vessels per unit length of channel (*veh* /*nm*), where nm stands for nautical miles;

Velocity (***u***), the average vessel speed per unit length of channel (knots or nautical miles per hour), where *kn* denotes knots or nautical miles per hour; and.

Intensity (***q***), the average number of vessels per unit time (*veh* /*h*).

According to these definitions, ***k***, ***q***, and ***u*** can be calculated as follows:

$$k = \frac{m}{X} \tag{1}$$

$$q = \frac{n}{T} \tag{2}$$

$$u = \frac{1}{m}\sum_{i=1}^{m} v_i \tag{3}$$

where ***m*** is the number of vessels at the observed moment, ***X*** is the length of observed channel, $\boldsymbol{v_i}$ is the speed of vessel ***i*** in the channel at the observed moment, ***n*** is the number of vessels passing the line of observation, and ***T*** is the duration over which the observations were made. These three variables have the following relationship:

$$q = k \cdot u \tag{4}$$

3.2. Empirical analysis

To calculate the three variables ***k***, ***q***, and ***u***, a time-space diagram is used (see Fig. 1a). The time-space diagram is an informative representation that illustrates vehicles' trajectories in the time-space dimension. The curves passing through the coordinates illustrate the trajectories of vessels, whereby the ordinate value of each point in the curve represents the distance to the channels' origin line (***x***), and the abscissa value of each point in the curve represents the observed time (***t***). The blue arrows in Fig. 1a (tangents of the curves) indicate the speed of each vessel when $t = t_0$. The red arrows in Fig. 1a indicate the speeds of the vessels when they pass the line of observation ($x = x_0$). According to Equations (1) and (2), ***X*** and ***T*** are required to calculate density, intensity, and velocity. In practice, we need a window of observation, as shown in Fig. 1b, to calculate the variables.

Because vessels are dynamic, the number of vessels in the channel is changing continuously for a given unit length of channel, ***X***. In other words, ***m*** is varying with time, set as ***m(t)***. Similarly, when the line of observation is placed in a different location, the number of vessels observed will be different during a given time duration ***T***. Therefore, *n* varies with distance, and is thus set as ***n(x)***. In conclusion, the following equations are used to calculate ***k***, ***q***, and ***u***:

$$k = \frac{\bar{m}}{X} = \frac{\frac{1}{T}\cdot\int_{t_0}^{t_0+T} m(t)dt}{X} = \frac{\int_{t_0}^{t_0+T} m(t)dt}{X\cdot T} \tag{5}$$

$$q = \frac{\bar{n}}{T} = \frac{\frac{1}{X}\cdot\int_{x_0}^{x_0+X} n(x)dx}{T} = \frac{\int_{x_0}^{x_0+X} n(x)dx}{X\cdot T} \tag{6}$$

$$u = \frac{q}{k} \tag{7}$$

where ***m(t)*** is the number of vessels in the channel ***X*** at time ***t***, ***n(x)*** is the number of vessels passing the line of observation ***x*** during time ***T***, and ***m (t)*** and ***n(x)*** are segmented and discontinuous functions, respectively. Providing that ***dt*** and ***dx*** are small enough (Fig. 1b), ***m(t)*** and ***n(x)*** can be counted. The velocity of a ship is lower than that of a car, and therefore we select $\boldsymbol{dt = 1\ s}$ and $\boldsymbol{dx = 0.0005\ nm}$. In this way, the observation window can be split into small slices, and ***m*** and ***n*** can be counted for each slice. The detail of calculating algorithm can be found in Algorithm 2.

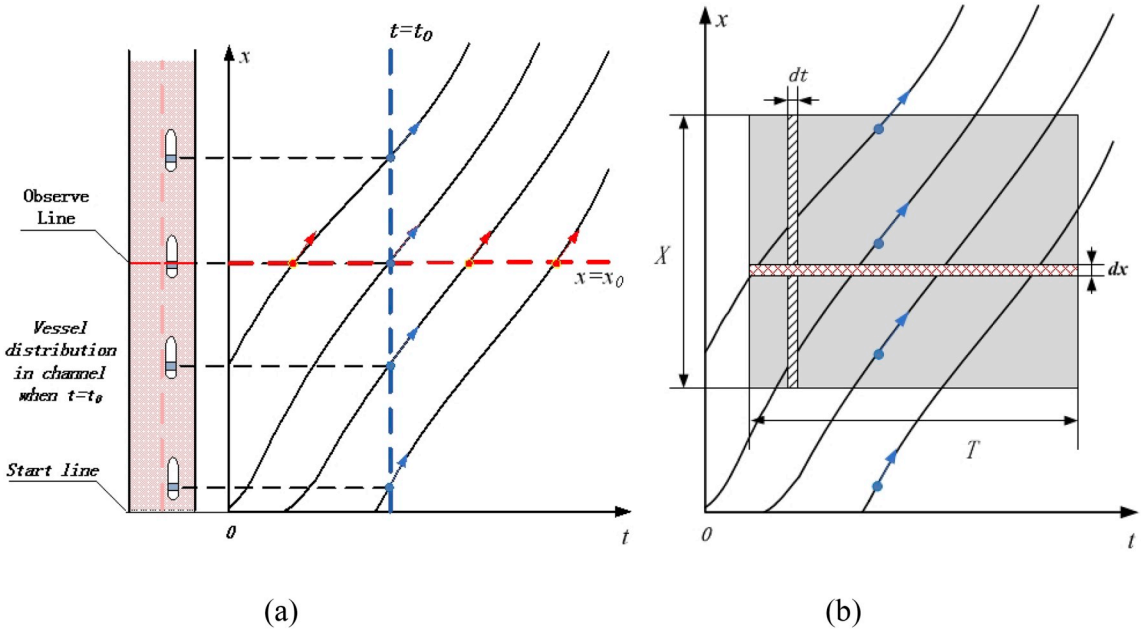

Fig. 1. A sketch map of the time-space diagram.

Algorithm 1. Gererate Ship flow w.r.t in given rectangle area (Area 1 or 2)

Algorithm 1: Generate Ship_flow w.r.t. in given rectangle area (Area 1 or 2)

Input : ship_trajectory: ship_traj; rectangle information: Area
Output : ship_flow
Notation: Area has four vertexes: A, B, C, D. edge AB and edge CD are long side. Each vertex is vector 2-by-1 vector.

```
// filter the data that is out of interesting area
if ship_traj is not crossing Area then return NaN;
// baseline of observing Area
E = 0.5* (A+D); F = 0.5* (B+C);
baseline = F-E; n = baseline/||baseline||_2;
// generate ship_flow data
while i<=ship_traj.length() do
    if Ship_flow(i) not in Area then
        ship_flow(i) = NaN;
        continue;
    P = ship_traj(i); vector = P-E;
    Length = InnerProduct(vector,n );
    ship_flow.t = ship_traj(i).t;
    ship_flow.x = Length
```

Algorithm 2. Calculation of traffic variables in each observing window

Algorithm 2: Calculation of traffic variables in each observing window

Input : ship flow data (ship_flow); observing data (ObsWin)
Output : q, k, u
Notation: ship_flow.t [sec], ship_flow.x = [NM]; ObsWin.t [sec], ObsWin.x [NM]

```
// boundary of observing window:
Bound.Up = max(ObsWin.x); Bound.Low = min(ObsWin.x);
Bound.Right = max(ObsWin.t); Bound.Left = min(ObsWin.t);
ObsWin.Area = (Bound.Up-Bound.Low)×( Bound.Right-Bound.Left);
// find the intersections of each ship trajectory and each edge of observing window
Crossing = polyxpoly(ship_flow.t, ship_flow.x, ObsWin.t, ObsWin.x);
// category the crossing points as inflow points and outflow points
OutFlow = Crossing(find(Crossing.x >= Bound.Up OR find(Crossing.t >= Bound.Right);
InFlow = Crossing(find(Crossing.x <= Bound.Low)) OR find(Crossing.t <= Bound.Left));
// total time spending in this window and total distance running in this window
dt = (sum(OutFlow.t) − sum(InFlow.t)) /3600;
dX = sum(OutFlow.x) − sum(InFlow.x);
// output results.
q = dX/(ObsWin.Area/3600);
k = dt/(ObsWin.Area/3600);
u = q/k;
```

3.3. Analysis procedures

Before the computing of traffic data, the study area and total observation duration should be chosen. The study area is chosen within the channel in which vessels sail. As we will repeat the computing for different groups of $\boldsymbol{k}$, $\boldsymbol{q}$ and $\boldsymbol{u}$, the total observation duration should be long enough for sufficient observations to be made. The specific procedures are as follows:

Step 1. Extract AIS data into trajectory information (see Fig. 2);

Step 2. Choose the study area in the channel of interest (where vessels are sailing) and the total duration over which observations are made;

Step 3. Set the start line in the observed channel (the entrance of the studied section);

Step 4. Filter the trajectories that are recorded in the observed channel, calculate the distance to the start line in the trajectory, and record the distance-time data (see Algorithm 1);

Step 5. Utilize the records in Step 4 to draw a time-space diagram (Fig. 3);

Step 6. Choose the observation window (**X** and **T**) as one sample;

Step 7. Calculate one group of values for the variables **k**, **q**, and **u** based on the procedure outlined in Section 3.1 Definition of variables (see Algorithm 2);

Step 8. Repeat Step 6, moving the observation window until the preset total observation duration is reached; and

Step 9. Draw the maritime traffic fundamental diagram using the sampled observations.

4. Data processing

4.1. Features of automatic identification system data

Greenshields (1934) used a camera to record road traffic. However, ships are much larger than cars, which makes it impossible to record ships' behaviour using a camera.

The AIS information contains static data [such as IMO number, call sign, ship name, and Maritime Mobile Service Identity (MMSI)] as well as dynamic data [such as Speed Over Ground (SOG), Course Over Ground (COG), position, and Coordinated Universal Time (UTC)]. The refresh rates of this information differ. The equipment transmits the

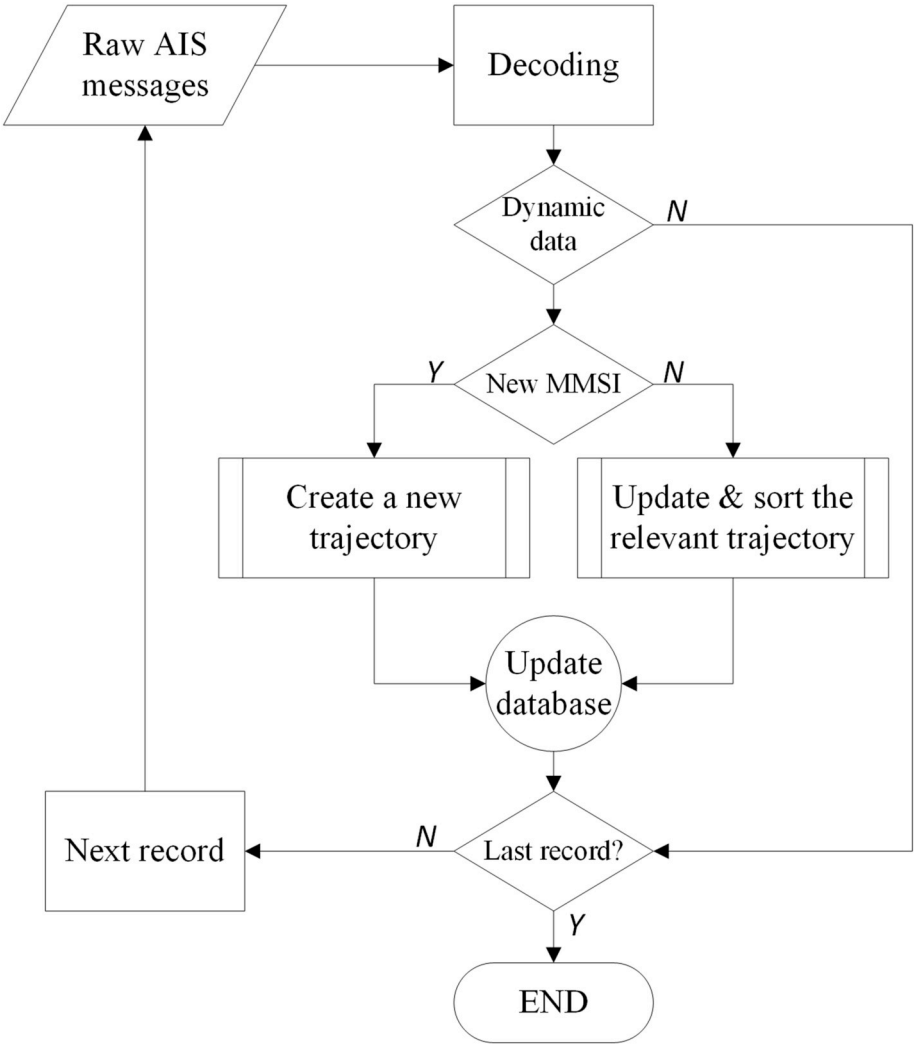

Fig. 2. The process of extracting AIS data.

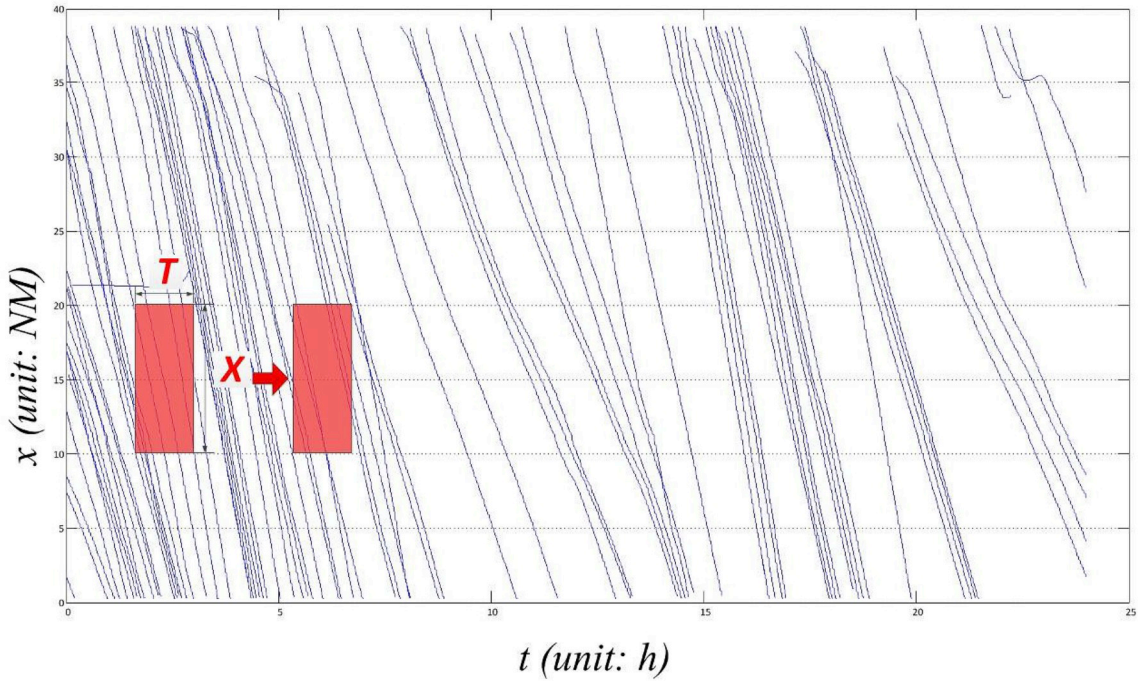

Fig. 3. Time-space diagram for the northern channel of Shanghai Port.

static information every 6 min, whereas the rate for dynamic information is more complicated. For anchoring ships, the broadcast rate is 3 min, and it increases to 2 s when the ship is sailing at high speed (ITU, 2010).

As a result, AIS data are obtained in near-real time at discrete points, but the refresh rate is asynchronous. To analyse the traffic fundamental relation, we need a continuous trajectory. Therefore, the raw AIS data first need to be processed. Noises exist in the AIS data and can adversely affect the results of analysis. To reduce the noises, we have removed some AIS data if (1) the same MMSI number appears at different positions in the same timeslot, or (2) the change of ship position in two successive timeslots exceeds the practical limit of ship speed (e.g. 50 knots), or (3) the speed in the record is too high (e.g. 50 knots).

The raw AIS was collected over the period of 1 January to 31 March (3 months) in 2010 and 2018. As the results of 2010 and 2018 are very similar, our discussion is based on 2010 mainly.

4.2. Ships' trajectories

Because an analysis of the traffic fundamental relationship needs only dynamic data, ships' static information can be ignored. The process for creating AIS history trajectories is illustrated in Fig. 2.

First, to read the AIS information, the raw data needed to be decoded. To decode the AIS data, we referred to the technical document "Recommendation ITU-R M.1371–4" (ITU, 2010). Second, to simplify the algorithm, we removed the pure static record. The information that included the dynamic data was transferred to the next step of the process. Third, the MMSI was extracted to search whether each MMSI had appeared previously; if "yes", then a new form was created to record the ship's new position and UTC, and if "no", then the new data were added to the relevant MMSI form and the new form was sorted by UTC. Fourth, the extracted AIS database was updated. If the current record was the final record, then the process was ended, otherwise the process moved to the next record and was continued.

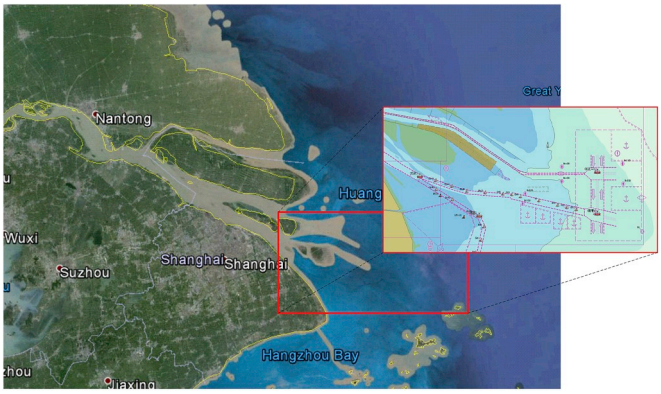

Fig. 4. A map of Shanghai Port.

After this process, the AIS data were stored in different forms, with the MMSI identifying each form and in each form the position data being sorted in order of increasing UTC. After this, the trajectories of ship movements were drawn. However, as the refresh rates are different, these trajectories are still discrete. Therefore, this paper uses a linear interpolation algorithm to increase the resolution of the trajectories.

4.3. Approach channels to Shanghai Port

To discover the maritime traffic fundamental relation, we chose Shanghai Port, one of the busiest ports in the world. Shanghai Port is located at the estuary of the Yangtze River. Therefore, the east-west-directed traffic (into and out of the Yangtze River) and north-south-directed traffic will cross at the estuary (see Fig. 4), which makes the Shanghai Port traffic flow complicated. There are only two channels through which Shanghai Port can be approached (Fig. 5). We chose these two channels to observe traffic data.

5. Empirical analysis

To ensure that the maritime fundamental diagram is portrayed correctly, we design several tests. We evaluate the influence of the different parameters (including $\boldsymbol{X}$ and $\boldsymbol{T}$), total observation times, observed channels, and observation dates on the final results. First, we define a basic sample group, the characteristics of which are given in Table 1. Fig. 6 shows two selected observed areas, namely, Area 1 and Area 2. Fig. 7 shows a time-space diagram of the traffic flow in Area 1 for the period 5–7 March 2010 & 5–7 March 2018-.

Fig. 8 displays the fundamental relationship as a series of scatterplots, with points being calculated based on the parameters set in Table 1. Fig. 8(1) shows the Fundamental diagram in 2010 and Fig. 8(1) shows that in 2018. As these two figure shown, with this parameter setting, maritime traffic flow has a similar fundamental relationship to that of highway traffic (see Fig. 14). The density-velocity relationship is near linear and negatively related. However, it is not ready to conclude

Table 1
The standard group.

Basic Sample Group				
Start Date	Observed area (see Fig. 6)	Total observed time	$\boldsymbol{X}$ (nm)	$\boldsymbol{T}$ (h)
5–7 March 2010 & 5–7 March 2018	Location (Area 1): Point A: 31.253725 N, 121.789511 E Point B: 31.175528 N, 121.868103 E Point C: 31.156647 N, 121.845886 E Point D: 31.233819 N, 121.764290 E	3 days	2	2

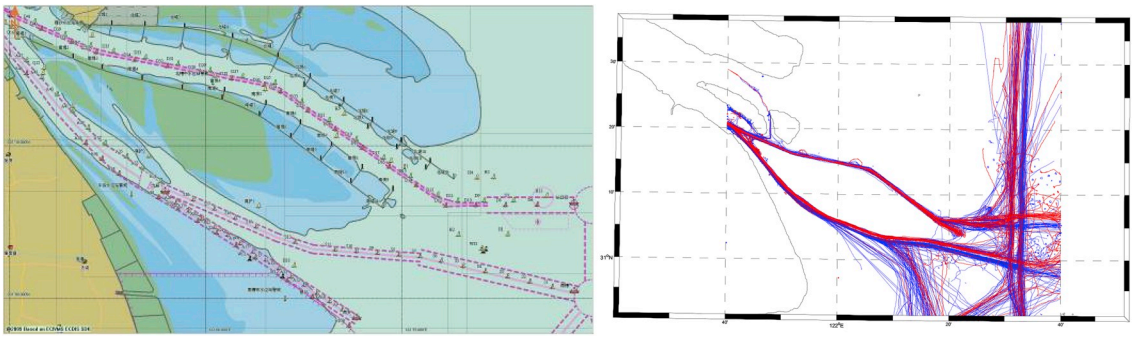

Fig. 5. Chart and AIS data of the Yangtze River estuary.

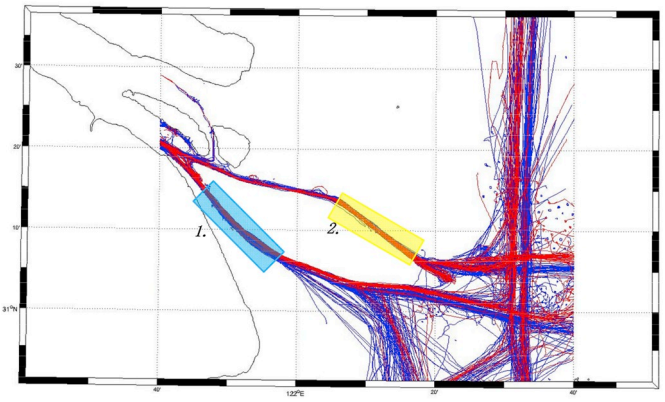

Fig. 6. Sketch map of two different channels.

whether these characteristics are a function only of the particular parameters. Therefore, in the following sections, we test the effect of different parameter settings on the fundamental relationship.

5.1. Test 1: the influence of different observation window size

In the road traffic flow situation, because the speed of traffic evaluation is high, the size of the observation window is small (e.g., 1 km and 1 min). The size of a ship is much larger than that of a car and the speed is much lower than that of a car. Therefore, we set the standard observation window as 2 nm and 2 *h*. To verify the size of the observation window, we test different observation window sizes. The size of the observation window for Control Group 1.1 (CG 1.1) is 3 nm and 2 *h*, and that for Control Group 1.2 (CG 1.2) is 2 nm and 4 *h*. The other parameters used for CG 1.1 and CG 1.2 are given in Table A1 in the Appendix. The results are shown in Fig. 9. Fig. 9 (1)–(2) show the fundamental diagrams in 2010 and Fig. 9 (3)–(4) shows the fundamental diagrams in 2018.

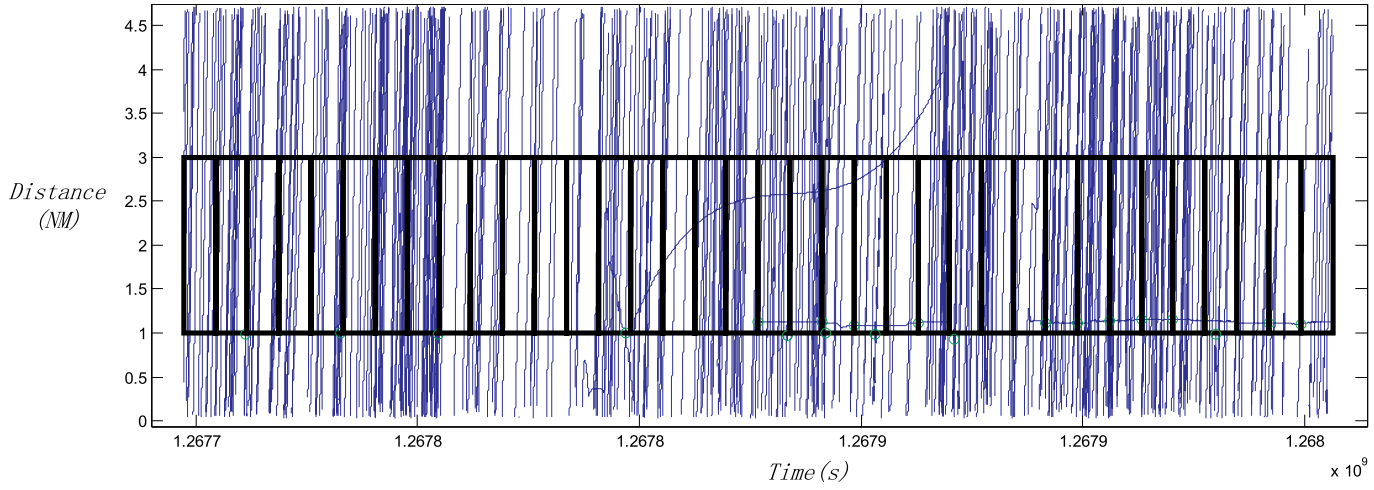

Fig. 7. Time-space diagram for maritime traffic.

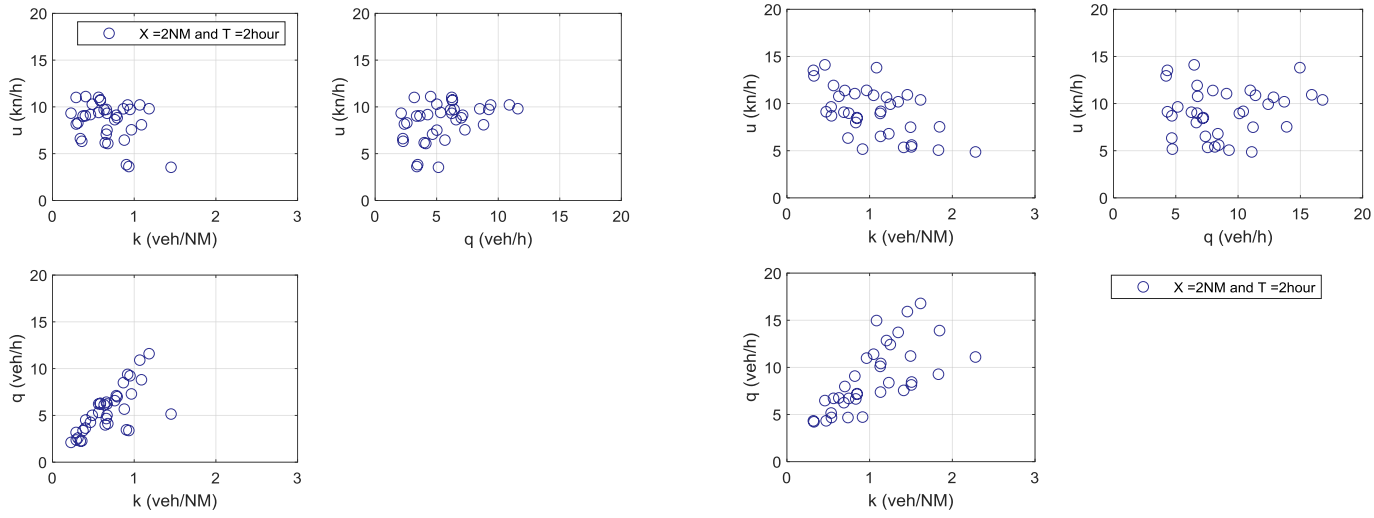

Fig. 8. Fundamental relationship diagrams for maritime traffic.

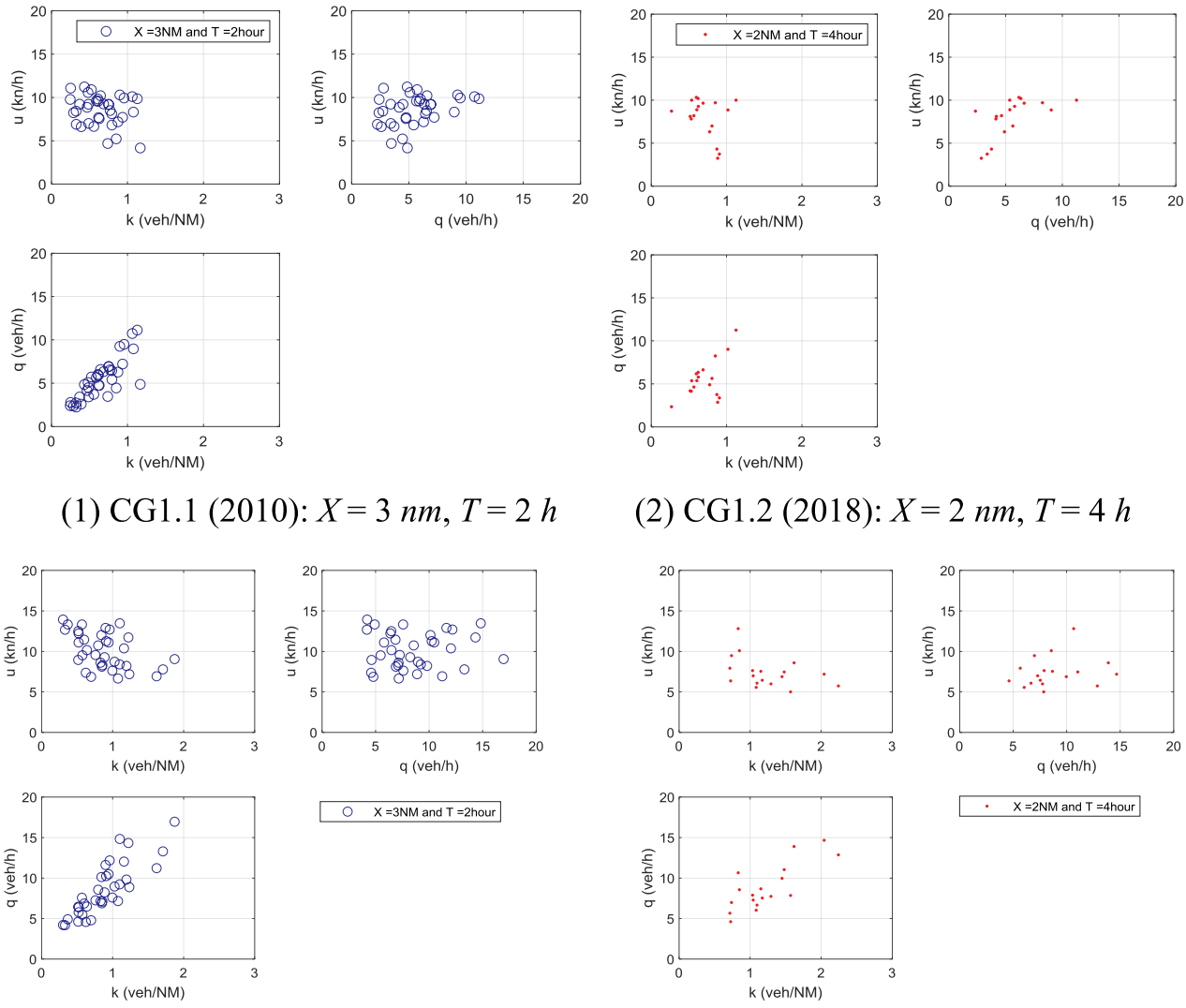

Fig. 9. Fundamental relationship diagrams for observation windows of different size.

5.2. Test 2: the influence of different total observed time

Because the observation window for the maritime situation is larger than that for highway traffic, we illustrate the effect of different total observed time on the fundamental relationship. For Control Group 2.1 (CG 2.1) the total observed time is 5 *days* and for CG 2.2 is 7 *days*. Details are shown in Table A2 in the Appendix. The results are shown in Fig. 10, in which it can be seen that although the greater number of days of observations provides more samples, the patterns of the fundamental diagrams for the two observation durations in the same year are very similar.

5.3. Test 3: the influence of different observation date

Maritime traffic should differ between different months. Therefore, we set four control groups with different observation dates: CG 3.1 on 1–3 January (Fig. 11(1) & Fig. 11(3)) and CG 3.2 on 1–3 February (Fig. 11(2) & Fig. 11(4)). Details are presented in Table A3.

5.4. Test 4: the influence of different channel

Traffic flow is likely to differ in different channels. For example, in Shanghai Port (Fig. 6), the Beicao channel (the northern channel) is the main channel for deep-draught vessels, and the depth of the channel is maintained at 10 m (after 2010, the maintained depth is 12.5 m), whereas the Nancao channel (the southern channel) is for smaller ships (Liu et al., 2014). We chose two areas in these channels for making observations (in Fig. 6, Area 1 and Area 2 are located in the Nancao channel and the Beicao channel, respectively). The settings of these experiments are shown in Table A4 and the fundamental diagrams for Area 2 are shown in Fig. 12.

5.5. Sensitivity test: the influence of observation time window

To test the influence from the size of observation window, different observation period have been chosen in this test. Therefore, we set 5 control groups with different time windows, such as 30min, 1 h, 4 h, 6 h, and 12 h. Similarly, the distance sensitivity analysis is also investigated. The alternative distances are 1 nm, 1.5 nm, 2.5 nm, 3 nm, and 3.5 nm. Since three primary parameters (***q, k, u***) are dependent such that the ***q*** is

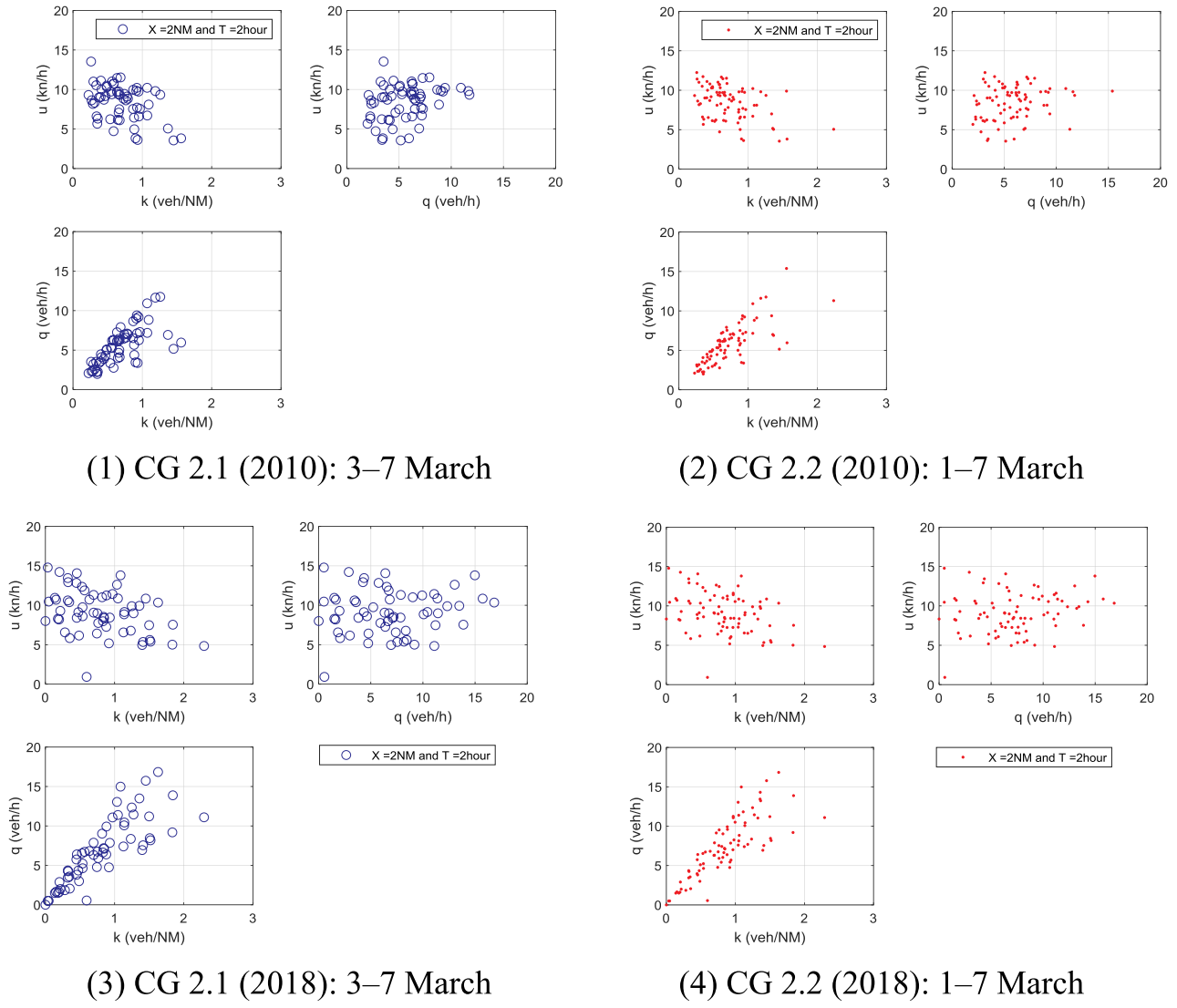

Fig. 10. Fundamental relationship diagrams for observation periods of different duration.

equal to ***k*** time ***u***, all the results of sensitivity tests are shown in the same plane, namely the density-flow plane. The settings can be found in Table A5 and the fundamental diagrams are shown in Fig. 13.

6. Discussion

6.1. Summary of empirical analysis

In Test 1, the different sizes of observation window have been set to determine their influences on the outcomes. As shown in Fig. 9 (1) CG 1.1 (2010), the different lengths of the distance window do not change the numbers of points, but the values of those. However, if we extend the observation time, the number of the observation points decreases, as shown in Fig. 9 (2) CG 1.2 (2010). In different observation windows, the value and the number of points change, but the shape of the points on each ***q-k-u*** plane is similar. A similar conclusion can be obtained when we see the data from 2018, i.e. Fig. 9 (3) and (4).

In Test 2, the different periods of time have been chosen. CG 2.1 (2010) and CG 2.1 (2018) show the result from 5 *days* observation. CG 2.2 (2010) and CG 2.2 (2018) show the outcomes from 7 *days*. By comparing with Figs. 8 and 10, it can be observed that although the values of the points in each fundamental diagram are different, the tendencies of these points are the same. On the ***k-u*** plane, the increasing traffic density will reduce the average speed. Moreover, on the ***k-q*** plane, the traffic density has a positive relationship with traffic flow. In Test 3, the different observation months have been chose. As the result shown, the values of points in each Figure are totally different, but the relationships between ***k-u*** and ***k-q*** are still the same.

In Test 4, the AIS data from another channel (Beicao Channel) have been analysed. Fig. 12 (1) shows that the fundamental relation between ***q-u-k*** in Beicao Channel in 2010 and Fig. 12 (2) shows that in 2018. By comparing Figs. 8 and 12, it can be found that the majority of traffic density in the Beicao channel is below 0.5 *veh/nm* which is lower than that in our standard group (Nancao Channel). In addition, the maximum speed in the Beicao channel is higher than that in the Nancao channel. This is because the Beicao channel is only for deep-draught ships, which are longer and need a longer safety distance between ships. Besides, the higher speed of these ships also requires a bigger gap between them, which will make traffic density decrease.

Test 5 shows the observation in various observation windows. Panel 1 of Fig. 13 shows the outcomes of different time windows. The red points represent the Control Groups with various time windows, and the blue one is the Standard Group (2 nm × 2 h). When the time window is shortened, more observation points are shown. In some windows, few or no ships are observed in the window, thus there are some points located in the origin ($k = 0$, $q = 0$) in Panel 1 of Fig. 13. Also, in some windows,

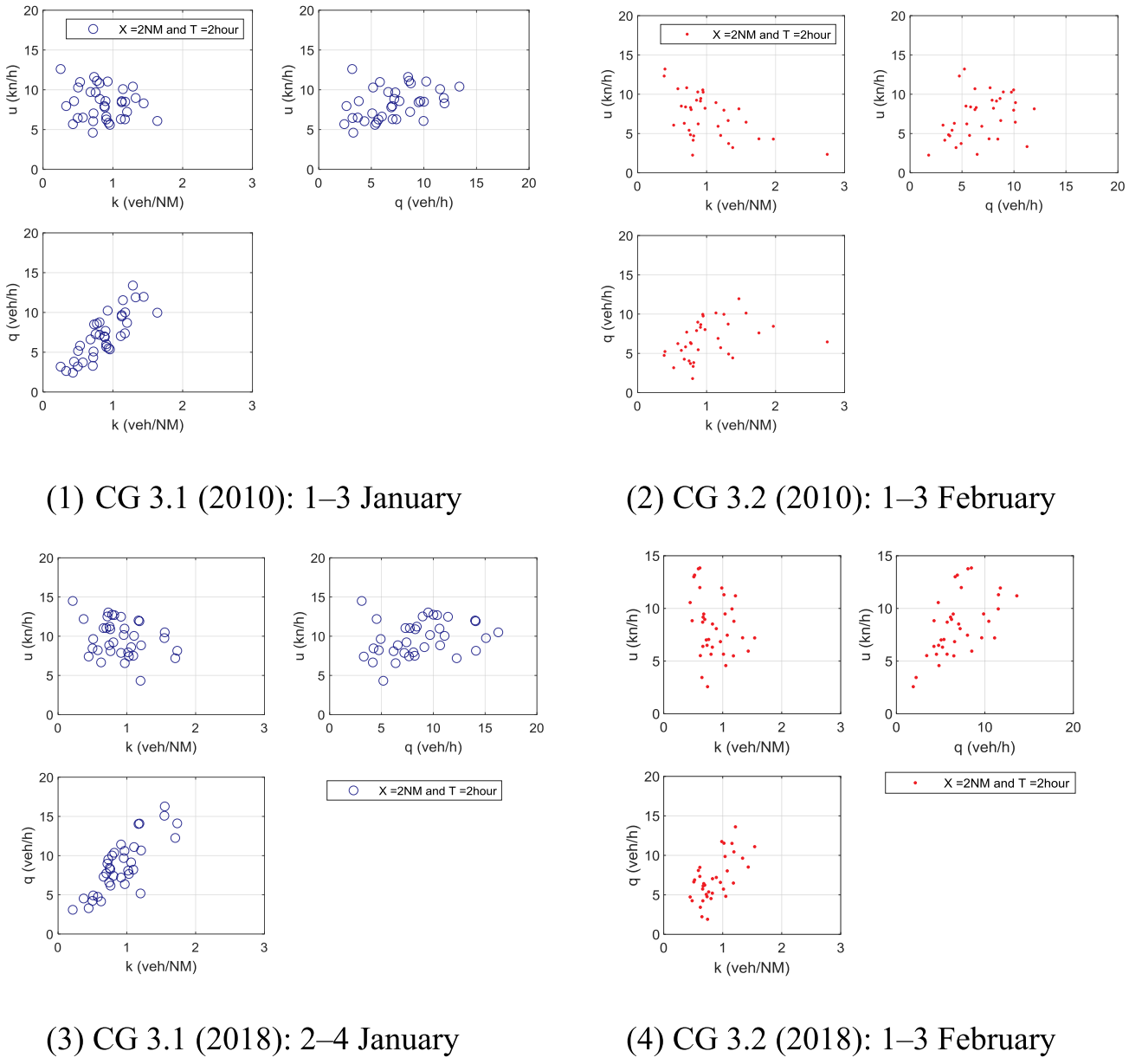

Fig. 11. The fundamental diagram for two different observation dates.

several ship at high speed is found, hence some points are located in high position ($k = 2$ *veh/nm*, $q = 20$ *veh/h*). With the time window gets enlarged, some points are merged. However, the linear positive relationships remained the same until the time window increase to 12*h* (only 6 points are showed in the figure). That means, in this case, the size of time windows will influence the number of the observation points in each fundamental diagram, but not the shape of the diagram.

Panel 2 of Fig. 13 shows the outcomes of different observed distance. When the distance window becomes longer, the value of the observation points changes. However, the linear relations between density and traffic flow are the same. That means, the length of the distance window will impact on the value of the points in the fundamental diagram, but the relations among fundamental parameters will not be affected.

From Test 1 to Test 5, we can see that, although the positions of points have been modified in different observation windows and different conditions, the envelopes of each figure in each year are similar. In density-speed (***k-u***) plane, with the increase of the density (***k***), the average velocity has a decreased tendency. While, in the density-flow (***k-q***) plane, it shows that the traffic flow has a positive relationship with traffic density.

6.2. *Marine traffic flow*

Greenshields (1934) proposed that the relationship between density and intensity is parabolic (Fig. 14*a*) and that between density and velocity is linear (Fig. 14*e*). Since the work of Greenshields, several types of fundamental relationship have been proposed. Daganzo (1994) proposed a bilinear (triangular) relationship in the density-intensity plane (Fig. 14 *b,f*), whereas Smulders (1990) constructed a parabolic-linear relationship (Fig. 14*c,g*). Drake et al. (1967) presented a totally non-linear fundamental relationship (Fig. 14*d,h*).

All these classical traffic flow models are developed for highway traffic flow. Comparing these models, we can find that, in density-speed plane (***k-u*** plane), the traffic density has a negative relation with traffic average speed; in density-flow plane (***k-q*** plane), with traffic density increases, the traffic flow will reach peak and after that the increase of traffic density will lead to the decrease of traffic flow. According to the relationship of ***k-q***, the states of traffic can be divided into two phases,

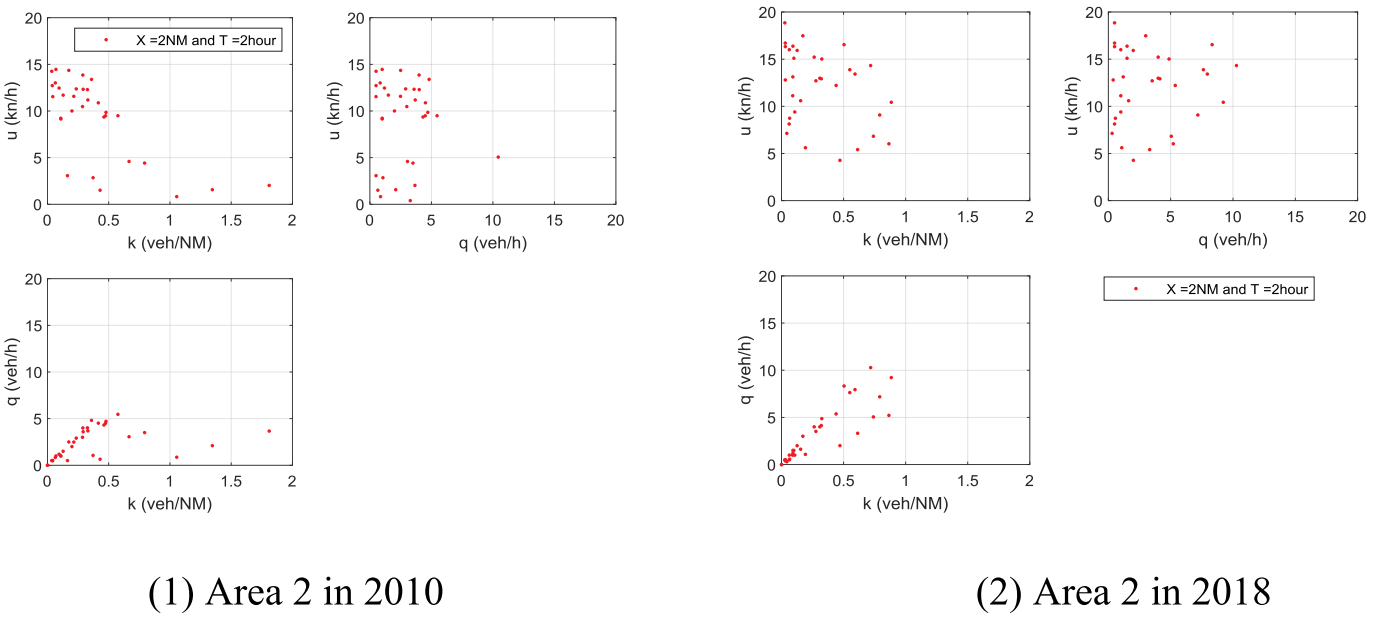

Fig. 12. The fundamental diagram for Area 2 (the Beicao channel).

namely free-flow and congested-flow.

Comparing the density-intensity and density-velocity planes between highway traffic and maritime traffic, we find that the fundamental relationship is similar, but still different. From our observations, we also find the negative relations between traffic density and speed on the ***k-u*** plane. Nevertheless, the traffic density only has a positive relationship with traffic flow. Although several points on the ***k-q*** plane as shown in Figs. 8–11 infer to the decreasing tendency, more observation points will be needed to confirm this tendency.

6.2.1. *Density-flow plane*

The density-flow plane (***k-q*** plane) of Fig. 8 shows that the observed marine traffic flow is in free-flow phase. In this phase, the maritime traffic density-intensity relationship is somewhat like the relationship proposed by Daganzo (1994): for low values of traffic density, the linear relationship between density and intensity is obvious; from these low values, traffic intensity increases to reach its peak at a density of around 1.0 *veh/nm* (Fig. 8). However, the declined tendency is missed.

Fig. 15 shows data and regression lines for the density-intensity relationship for the Nancao channel by utilizing the maritime fundamental relationship data in Fig. 8. The data on the density-intensity plane of Fig. 15 can be proposed as classical models, namely Greenshields, Greenberg, Underwood, and Pipes (Underwood, 1961; Kang et al., 2018). The models and results of regressions are shown in Table 2. The density-flow relationship of marine traffic is very much similar to the relationship defined by classical models. The empirical findings confirm that a vessel moves like free-flow traffic. However, vessel may slow down if she becomes too close to each other, and vessels interact with other vessels when ship domains overlap. The ship domain theory has been adopted to determine the probability of ship collision with bridge structures (IABSE, 1993). Our study provides empirical evidence for a rigorous link between classical models in the highway traffic literature and the ship domain theory in the marine traffic literature.

6.2.2. *Density-velocity plane*

Density and velocity have a negative correlation in maritime traffic, which is similar to that observed for highway traffic flow. Various models have been developed to describe the fundamental relationship for highway traffic flow. Table 3 and Fig. 16 report the traffic flow according to classical models, namely Greenshields, Greenberg, Underwood, and Pipes. The *R*-squared shows that the classical models cannot fit the data satisfactorily.

6.3. *Handling the errors in AIS data*

Since AIS data is the data source of this analysis, thus the quality of AIS data is very critical. During the analysis, two main sources of errors might occur, and they are discussed in the following.

Source 1: the errors in raw AIS data. AIS messages are inevitable containing various errors, especially 50% of human inputted information might have errors (Harati-Mokhtari et al., 2007). The position information is usually relying on GPS onboard and this type of data contains three error sources: (1) errors in onboard equipment, (2) errors due to transmission, and (3) errors in storage in receivers. Since we do not know the real position of the ship at each moment, thus this type of errors is difficult to validate. However, we can filter some obvious errors to clean the data, i.e. a same MMSI name might not appear at different position at the same time; the speed of the merchant ship usually is less than 50 knots.

Source 2: during the statistical process, some errors might be added. Firstly, the AIS signal is missing in a long period of time in which the ship might finish its previous voyage or other unknown activities. Thus, we have split one trajectory into to two, provided that the relative distance between two records is exceeding 12 [NM] (much bigger than observing window), and the time difference between two neighbouring records exceeding 1200 [sec]. Secondly, we project the 2 dimensional ship trajectory (longitude and latitude of the ship) into 1 dimension (distance to observe line), which contains errors. In the highway traffic flow, cars are moving within a regular lane and the width of lane contains one car only. Thus, the trajectory of cars is almost the centre-line of the lane. However, in the maritime traffic, channel is often wide enough to contain more than one ships and the ship's trajectory might not completely follow the central-line of waterways. Thus, when we project the 2D data into 1D, some errors are inevitably contained.

Since AIS is our only and the best data source, it is difficult to calculate the errors rate containing in AIS data. However, we might imply the error rate, when we observe some abnormal behaviours, such as the shake of ship positions in time-space diagram. An example is shown in the left panel of Fig. 17 in which a "z" shaped path is observed. However according to the neighbouring data, the ship should sail smoothly. This abnormal behaviour might occur owing to the two main reasons discussed previously. We use the percentage of position shake to

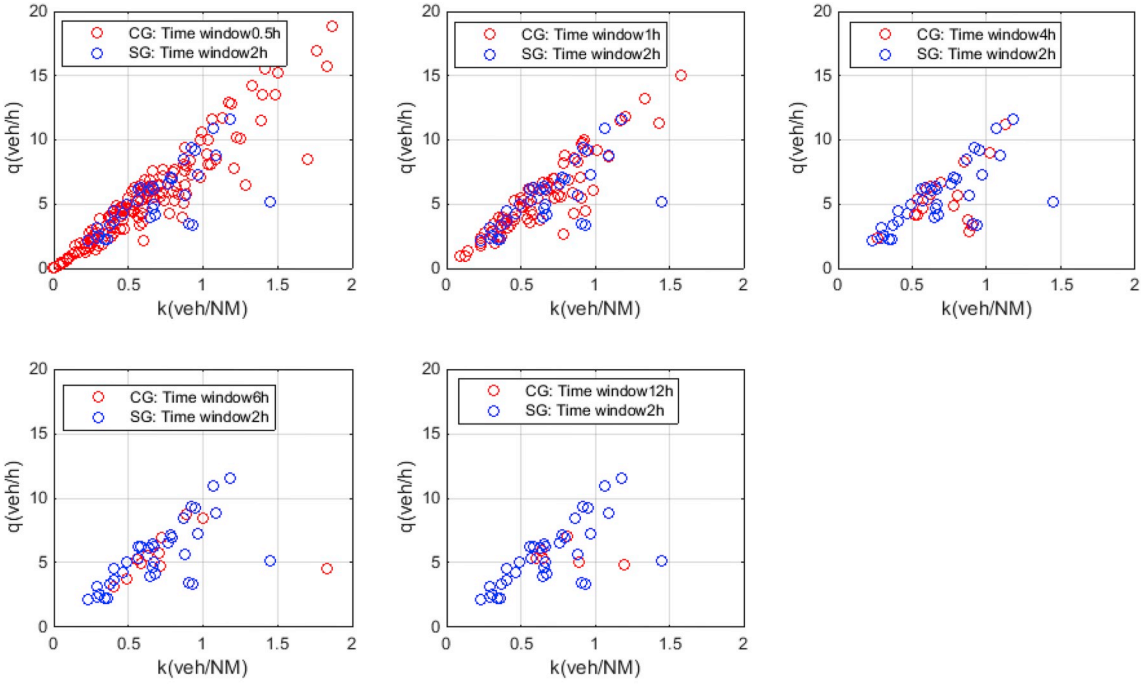

(1) Sensitivity of time-window

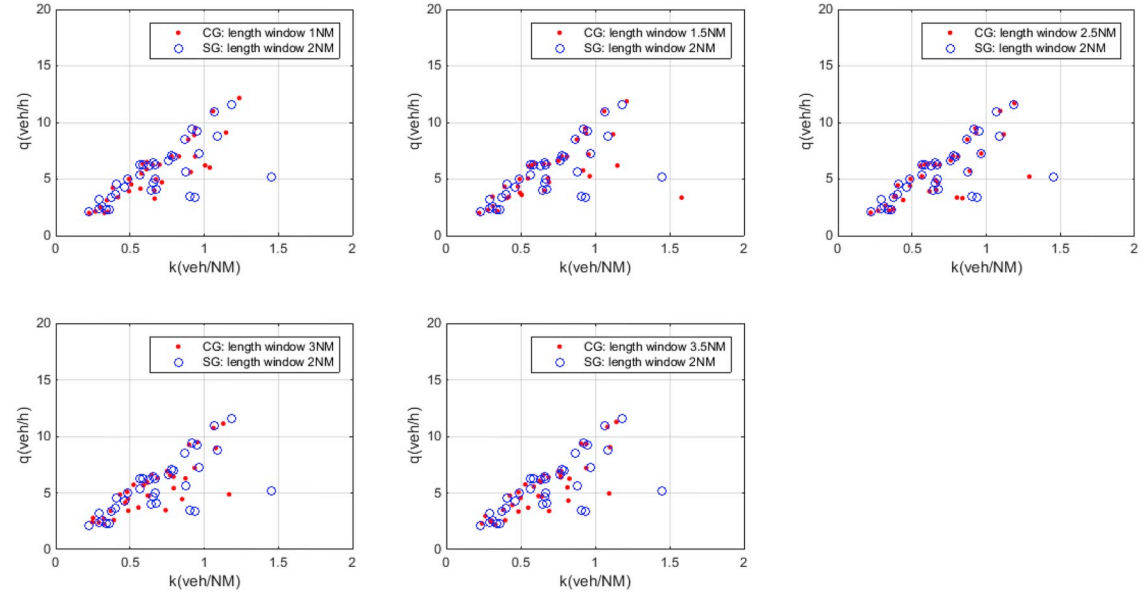

(2) Sensitivity of distance-window

Fig. 13. The fundamental diagrams for sensitivity test.

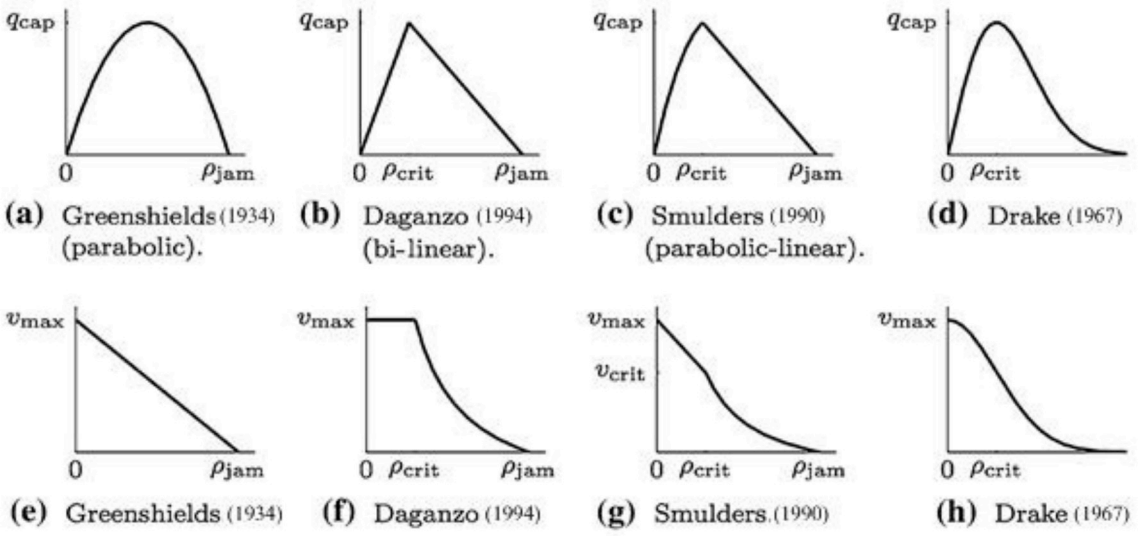

Fig. 14. Different shapes of the highway traffic fundamental relationship.

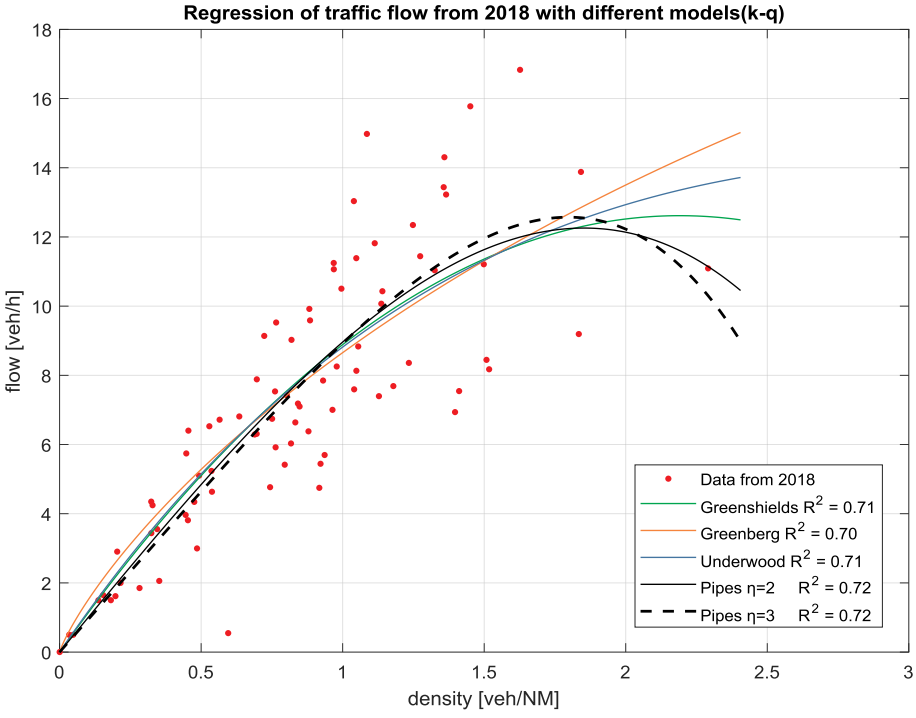

Fig. 15. The regression equation for maritime traffic flow.

Table 2
Regression comparison on the density-flow plan.

Model	Equation	Coefficients	(95% confidence bounds)	R-squared
Greenshields	f(k) = a*k^2 + b*k	a1 = −2.629 (−3.678, −1.579)	vf = 11.52 (10.11, 12.92)	0.7128
Greenberg	f(k) = a2*k-v0*k*log(k)	a2 = 8.656 (8.132, 9.18)	v0 = 2.748 (1.487, 4.009)	0.6957
Underwood	f(k) = exp (log(k)+a3-(1/k0)*k)	a3 = 2.487 (2.319, 2.655)	k0 = 3.226 (1.793, 4.659)	0.7077
Pipes (η = 2)	f(k) = vf*k-a4*(k)^3	a4 = 0.9645 (0.5961, 1.333)	vf = 9.926 (9.122, 10.73)	0.7189
Pipes (η = 3)	f(k) = vf*k-a4*(k)^4	a4 = 0.4017 (0.2471, 0.5562)	vf = 9.326 (8.693, 9.96)	0.7179

Table 3
Regression comparison on the density-velocity plan.

Model	Equation	Coefficients	(95% confidence bounds)	R-squared
Greenshields	f(k) = vf – a1*k	a1 = 2.049 (0.895, 3.202)	vf = 10.83 (9.721, 11.93)	0.1321
Greenberg	f(k) = a2 – v0*log(k)	a2 = 8.883 (8.294, 9.471)	v0 = 0.4719 (−0.003866, 0.9477)	0.04533
Underwood	f(k) = exp (a3-(1/k0)*k)	a3 = 2.392 (2.277, 2.506)	k0 = 4.472 (1.84, 7.104)	0.1291
Pipes ($\eta = 2$)	f(k) = vf-a4*(k)^2	a4 = 1.028 (0.4427, 1.613)	vf = 10.04 (9.29, 10.79)	0.1296
Pipes ($\eta = 3$)	f(k) = vf-a4*(k)^3	a4 = 0.498 (0.1955, 0.8005)	vf = 9.673 (9.04, 10.31)	0.1157

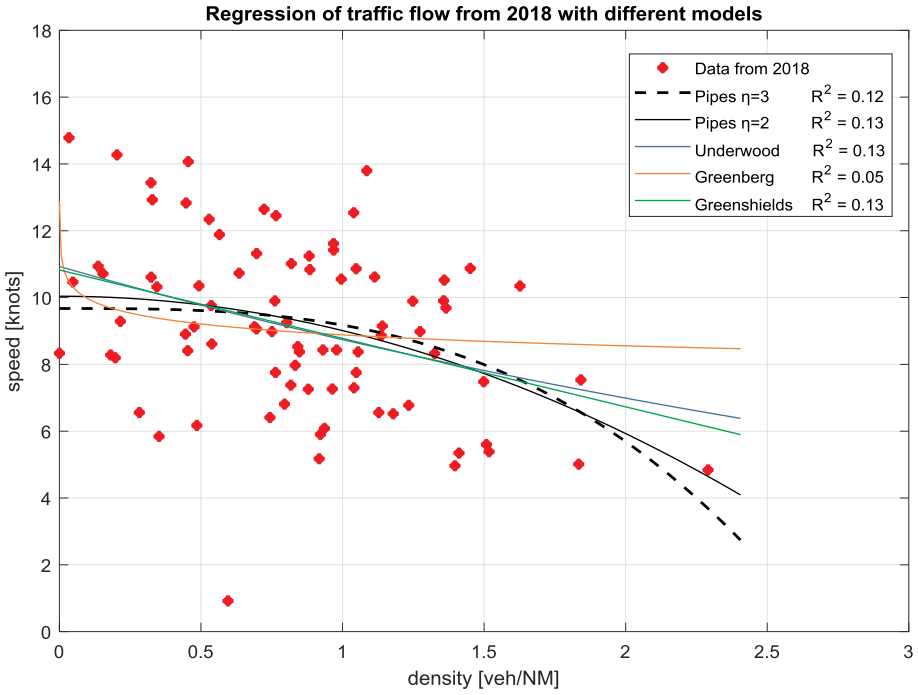

Fig. 16. Data and regression lines for the density-velocity relationship.

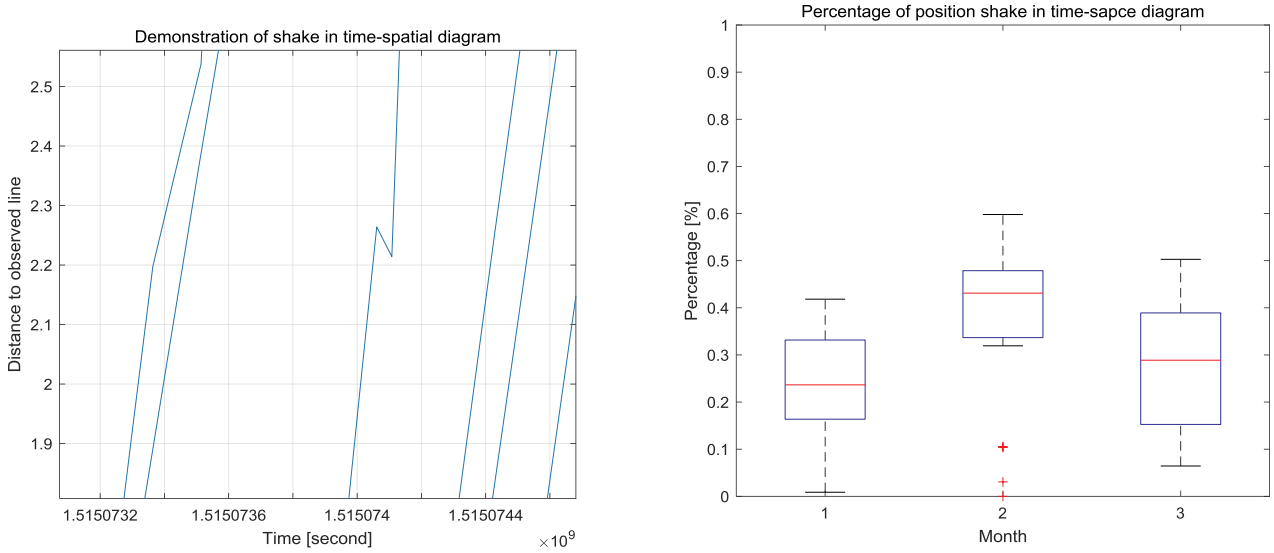

Fig. 17. A demonstrate of position shake in time-space diagram and its percentage in each month.

represent the error rate of the collected data in this manuscript. If one path in time-space diagram contains a "z" shaped shake, we count the while path is abnormal. In return, the error rate in each month is presented. In January and March, the error rate is relatively low and the average is approximately 0.2 and 0.3. In February, the error is relatively high which is approximately 0.4.

To reduce errors and obtain more reliable results, we expect some developments on the reliability of AIS equipment (Source I) and a better statistical tool that does not need to reduce 2D data into 1 D (Source II), e.g. pedestrian traffic flow techniques (Vanumu et al., 2017).

7. Conclusions

The fundamental relationship is the foundation of traffic flow theory and of the macroscopic traffic model. Therefore, the maritime fundamental relationship needs to be considered before developing a maritime traffic flow model. Here, we have quantified the fundamental relationship of maritime traffic flow by using Shanghai Port AIS data. We have used the maritime time-space diagram with various parameter settings to represent vessel traffic. We have performed regressions on the traffic model data to quantify the observed patterns on the density-flow plan and on the density-velocity plan.

The results show that marine traffic flow is very similar to highway traffic flow but does not fully fit any existing known fundamental relationships. The density-intensity relationship of marine traffic is very much similar to the relationship defined by classical models, while the density-speed relationship seemly not similar to the classical models. The difference observed might be due to the difference between highway traffic flow and ship traffic flow. For instance, the ship traffic does not have physical boundary of lanes and the overtaking is common. These differences might result in the discrepancy between the classical models and the ship traffic data. Such understanding is important to develop a passage planning system in ports to regulate marine traffic in ports (Yip, 2015). Modifications in analyses might be needed for the further studies, in which we might refer to some achievements in, for example, pedestrian traffic flow (Vanumu et al., 2017). Moreover, although we have made substantial effort to eliminate possible bias, we expect the further empirical studies on this theme for ship traffic flow will advance to further eliminate bias.

This study, however, has several limitations and also suggests opportunities for future investigations. First, the analysis ignores the variation of the ship sizes. As the ship size varies greatly compared with the vehicle in the surface transportation, the fundamental diagrams that determined the character of relative motions of ships should be related to a primary quantity. Second, our study does not consider any theoretical fundamental diagram. Incorporating theoretical analysis may result in deeper understanding of marine traffic flow. Thirdly, a way to reduce the errors in AIS data and statistical analysis needs further investigation. Finally, further applications of the fundamental diagram should be explored, such as finding the capacity drop point in real traffic flow, estimating the maximum capacity of a specific waterway, and forecasting the traffic status.

Acknowledgements

The study was partially supported by grants from the Research Grants Council of the Hong Kong Special Administrative Region, China (Project No. PolyU 5300/12E), the National Science Foundation of China (NSFC) through Grant No. 51679180, and the National Key R&D Program of China through Grant No. 2018YFC1407405. The authors acknowledge the anonymous referees for their valuable comments and suggestion on previous version of this article.

Appendix A. Supplementary data

Supplementary data to this article can be found online at https://doi.org/10.1016/j.oceaneng.2019.106195.

Appendix

Table A1
Parameters in the control groups for test 1.

Start Date	Observed area	Total observed time	***X (nm)***	***T (h)***
Control Group 1.1 (2010) & (2018)				
5–7 March 2010 & 2018	Location: Point A: 31.253725 ***N***, 121.789511 ***E*** Point B: 31.175528 ***N***, 121.868103 ***E*** Point C: 31.156647 ***N***, 121.845886 ***E*** Point D: 31.233819 ***N***, 121.764290 ***E***	3 days	**3**	2
Control Group 1.2 (2010) & (2018)				
Start Date	Observed area	Total observed time	***X (nm)***	***T (h)***
5–7 March 2010 & 2018	Location: Point A: 31.253725 ***N***, 121.789511 ***E*** Point B: 31.175528 ***N***, 121.868103 ***E*** Point C: 31.156647 ***N***, 121.845886 ***E*** Point D: 31.233819 ***N***, 121.764290 ***E***	3 days	2	**4**

Table A2
Parameters in the control groups for test 2.

Control Group 2.1 (2010) & (2018)				
Start Date	Observed area	Total observed time	***X (nm)***	***T (h)***
3–7 March 2010 & 2018	Location: Point A: 31.253725 ***N***, 121.789511 ***E*** Point B: 31.175528 ***N***, 121.868103 ***E*** Point C: 31.156647 ***N***, 121.845886 ***E*** Point D: 31.233819 ***N***, 121.764290 ***E***	**5 days**	2	2
Control Group 2.2 (2010) & (2018)				
Start Date	Observed area	Total observed time	***X (nm)***	***T (h)***
1–7 March 2010 & 2018	Location: Point A: 31.253725 ***N***, 121.789511 ***E*** Point B: 31.175528 ***N***, 121.868103 ***E*** Point C: 31.156647 ***N***, 121.845886 ***E*** Point D: 31.233819 ***N***, 121.764290 ***E***	**7 days**	2	2

Table A3
Parameters in the control groups for test 3.

Control Group 3.1 (2010) & (2018)				
Start Date	Observed area	Total observed time	***X* (nm)**	***T* (h)**
1–3 January 2010 & 2018	Location: Point A: 31.253725 ***N***, 121.789511 ***E*** Point B: 31.175528 ***N***, 121.868103 ***E*** Point C: 31.156647 ***N***, 121.845886 ***E*** Point D: 31.233819 ***N***, 121.764290 ***E***	3 days	2	2
Control Group 3.2 (2010) & (2018)				
Start Date	Observed area	Total observed time	***X* (nm)**	***T* (h)**
1–3 February 2010 & 2018	Location: Point A: 31.253725 ***N***, 121.789511 ***E*** Point B: 31.175528 ***N***, 121.868103 ***E*** Point C: 31.156647 ***N***, 121.845886 ***E*** Point D: 31.233819 ***N***, 121.764290 ***E***	3 days	2	2

Table A4
Parameters in the control groups for test 4.

Control Group 4.1 (2010) & (2018)				
Start Date	Observed area	Total observed time	***X* (nm)**	***T* (h)**
5–7 March 2010& 2018	**Location 2:** Point A: 31.233433 ***N***, 122.117033 ***E*** Point B: 31.142661 ***N***, 122.258128 ***E*** Point C: 31.112000 ***N***, 122.258128 ***E*** Point D: 31.200000 ***N***, 122.117033 ***E***	3 days	2	2
Control Group 4.2 (2010) & (2018)				
Start Date	Observed area	Total observed time	***X* (nm)**	***T* (h)**
4–6 March 2010 & 2018	**Location 2:** Point A: 31.233433 ***N***, 122.117033 ***E*** Point B: 31.142661 ***N***, 122.258128 ***E*** Point C: 31.112000 ***N***, 122.258128 ***E*** Point D: 31.200000 ***N***, 122.117033 ***E***	3 days	2	2

Table A5
(1) Parameters in the control groups for time sensitivity test.

Control Group	Start Date	Observed area	Total observed time	*X* (nm)	*T* (h)
CG 5.1	**5–7 March 2010**	Point A: 31.253725 ***N***, 121.789511 ***E***	3 days	2	0.5
CG 5.2		Point B: 31.175528 ***N***, 121.868103 ***E***			1
CG 5.3		Point C: 31.156647 ***N***, 121.845886 ***E***			4
CG 5.4		Point D: 31.233819 ***N***, 121.764290 ***E***			6
CG 5.5					12

Table A5.(2) Parameters in the control groups for distance sensitivity test.

CG 5.1	**5–7 March 2010**	Point A: 31.253725 ***N***, 121.789511 ***E***	3 days	1	2
CG 5.2		Point B: 31.175528 ***N***, 121.868103 ***E***		1.5	
CG 5.3		Point C: 31.156647 ***N***, 121.845886 ***E***		2.5	
CG 5.4		Point D: 31.233819 ***N***, 121.764290 ***E***		3	
CG 5.5				3.5	

References

Bando, M., Hasebe, K., Nakayama, A., Shibata, A., Sugiyama, Y., 1995. Dynamical model of traffic congestion and numerical simulation. Phys. Rev. E - Stat. Nonlinear Soft Matter Phys. 51, 1035–1042.

Buckley, D.J., 1968. A semi-Poisson model of traffic flow. Transport. Sci. 2 (2), 107–133.

Chen, Z., Xue, J., Wu, C., Qin, L.Q., Liu, L., Cheng, X., 2018. Classification of vessel motion pattern in inland waterways based on Automatic Identification System. Ocean Eng. 161, 69–76.

Daganzo, C.F., 1994. The cell transmission model: a dynamic representation of highway traffic consistent with the hydrodynamic theory. Transp. Res. Part B Methodol. 28 (4), 269–287.

Drake, J.S., Schofer, J.L., May, A.D., 1967. A statistical analysis of speed-density hypotheses. Highw. Res. Rec. 154, 53–87.

Feng, H., 2013. Cellular automata ship traffic flow model considering integrated bridge system. Int. J. u- e-Serv. Sci. Technol. 6 (6), 121–132.

Gipps, P.G., 1981. A behavioural car-following model for computer simulation. Transp. Res. Part B Methodol. 15 (2), 105–111.

Greenshields, B.D., 1934. The photographic method of studying traffic behaviour. In: Proceedings of the 13th Annual Meeting of the Highway Research Board, pp. 382–399.

Harati-Mokhtari, A., Wall, A., Brooks, P., Wang, J., 2007. Automatic identification system (AIS): data reliability and human error implications. J. Navig. 60 (3), 373–389.

He, L., Jiang, Y., Yin, Z., Zhou, B., Tang, H., 2012. Following distance model of inland ship. J. Traffic Transp. Eng. 12 (1), 55–62 (In Chinese).

Hongxiang, F., Xiongguan, B., Jianghua, Z., Song, L., Qionglin, F., 2015. Cellular automata model on AIS-based for variable two-way waterway. J. Ind. Eng. Manag. 8 (3) https://doi.org/10.3926/jiem.1347.

Hou, H.Q., Li, Y.C., He, W., Liu, X.L., 2014. Vessel traffic flow distribution model of bridge area waterway in the middle stream of Yangtze River. Appl. Mech. Mater. 551, 127–133.

IABSE, 1993. Ship Collision with Bridges: the Interaction between Vessel Traffic and Bridge Structures. International Association for Bridge and Structural Engineering, Switzerland.

ITU, 2010. Technical characteristics for an automatic identification system using time-division multiple access in the VHF maritime mobile band. In: Union, I.T. (Ed.). M.1371-1374.

Jagerman, D.L., Altiok, T., 2003. Vessel arrival process and queueing in marine ports handling bulk materials. Queue. Syst. Theor. Appl. 45 (3), 223–243.

Jensen, T.K., Hansen, M.G., Lehn-Schiøler, T., Melchild, K., Rasmussen, F.M., Ennemark, F., 2013. Free flow-efficiency of a one-way traffic lane between two pylons. J. Navig. 66 (06), 941–951.

Kang, L., Meng, Q., Liu, Q., 2018. Fundamental diagram of ship traffic in the Singapore Strait. Ocean Eng. 147, 340–354. https://doi.org/10.1016/j.oceaneng.2017.10.051.

Kasyk, L., Kijewska, M., 2013. Gumbel distribution in analysis of vessel speed on the Świnoujście–Szczecin fairway. Zeszyty Naukowe/Akademia Morska w Szczecinie 36 (108), 85–89.
Köse, E., Başar, E., Demirci, E., Güneroğlu, A., Erkebay, Ş., 2003. Simulation of marine traffic in Istanbul Strait. Simulat. Model. Pract. Theor. 11 (7–8), 597–608.
Li, S., Meng, Q., Qu, X., 2012. An overview of maritime waterway quantitative risk assessment models. Risk Anal. 32 (3), 496–512. https://doi.org/10.1111/j.1539-6924.2011.01697.x.
Lighthill, M.J., Whitham, G.B., 1955. On kinematic waves I: flood movement in long rivers. Proc. R. Soc. A Math. Phys. Eng. Sci. 229 (1178), 281–316.
Lighthill, M.J., Whitham, G.B., 1955. On kinematic waves II: a theory of traffic flow on long crowded roads. Proc. R. Soc. A Math. Phys. Eng. Sci. 229 (1178), 317–345.
Liu, J, Cheng, H., Zhao, D., 2014. Siltation characteristics of the 12.5m deepwater navigation channel in Yangtze estuary (in Chinese). Adv. Water Sci. 25 (3), 358–365.
Mahnke, R., Kuhne, R., 2007. Probabilistic description of traffic breakdown. In: Schadschneider, A., Pöschel, T., Kuhne, R., Schreckenberg, M., Wolf, D.E. (Eds.), Traffic and Granular Flow '05. Springer, New York, pp. 527–536.
Merrick, J.R., van Dorp, J.R., Dinesh, V., 2005. Assessing uncertainty in simulation-based maritime risk assessment. Risk Anal. 25 (3), 731–743. https://doi.org/10.1111/j.1539-6924.2005.00616.x.
Nagel, K., Schreckenberg, M., 1992. A cellular automaton model for freeway traffic. J. Phys. Archiv. 2 (12), 2221–2229.
Payne, H.J., 1971. Models of freeway traffic and control. In: Mathematical Models of Public Systems. Simulation Council Proceedings, pp. 51–61.
Prigogine, I., 1961. A Boltzmann-like approach to the statistical theory of traffic flow. In: Herman, R. (Ed.), *Theory Traffic Flow 1959*, Proceedings. Elsevier, Amsterdam, pp. 158–164.
Qi, L., Zheng, Z., Gang, L., 2017. A cellular automaton model for ship traffic flow in waterways. Phys. Stat. Mech. Appl. 471, 705–717. https://doi.org/10.1016/j.physa.2016.12.028.
Qi, L., Zheng, Z., Gang, L., 2017. Marine traffic model based on cellular automaton: considering the change of the ship's velocity under the influence of the weather and sea. Phys. Stat. Mech. Appl. 483, 480–494. https://doi.org/10.1016/j.physa.2017.04.125.
Qian, X., 2009. Application of Macroscopic Fundamental Diagrams to Dynamic Traffic Management. Master of Science. Delft University of Technology.
Richards, P.I., 1956. Shock waves on the highway. Oper. Res. 4 (1), 42–51.
Smulders, S., 1990. Control of freeway traffic flow by variable speed signs. Transp. Res. Part B Methodol. 24 (2), 111–132.
Underwood, R.T., 1961. Speed, Volume and Density Relationships: Quality and Theory of Traffic Flow. Yale Bureau of Highway Traffic, pp. 141–188.
van Wageningen-Kessels, F., van Lint, H., Vuik, K., Hoogendoorn, S., 2014. Genealogy of traffic flow models. EURO J. Transp. Logist. 4 (4), 445–473.
Vanumu, L.D., Rao, K.R., Tiwari, G., 2017. Fundamental diagrams of pedestrian flow characteristics: a review. Eur. Trans. Res. Rev. 9 (49), 1–13.
Wen, Y., Huang, Y., Zhou, C., Yang, J., Xiao, C., Wu, X., 2015. Modelling of marine traffic flow complexity. Ocean Eng. 104, 500–510. https://doi.org/10.1016/j.oceaneng.2015.04.051.
Wiedemann, R., 1974. Simulation des Strassenverkehrsflusses. Institute for Traffic Engineering, University of Karlsruhe (Tech. Rep).
Xiao, F., Ligteringen, H., van Gulijk, C., Ale, B., 2015. Comparison study on AIS data of ship traffic behavior. Ocean Eng. 95, 84–93. https://doi.org/10.1016/j.oceaneng.2014.11.020.
Xu, W., Chu, X., Chen, X., Li, Y., 2013. Method of generating simulation vessel traffic flow in the bridge areas waterway. In: 2013 International Conference on Computer Sciences and Applications. IEEE, pp. 808–812.
Yip, T.L., 2013. A marine traffic flow model. TransNav: Int. J. Mar. Navig. Saf. Sea Transp. 7 (1), 109–113.
Yip, T.L., 2015. Passage planning system in ports. TransNav: Int. J. Mar. Navig. Saf. Sea Transp. 9 (4), 483–487.
Zhou, Y., Daamen, W., Vellinga, T., Hoogendoorn, S.P., 2019. Ship classification based on ship behavior clustering from AIS data. Ocean Eng. 175, 176–187. https://doi.org/10.1016/j.oceaneng.2019.02.005.
Zhu, J., Zhang, W., 2009. Calculation model of inland waterway transit capacity based on ship-following theory. J. Traffic Transp. Eng. 9 (5), 83–87 (In Chinese).

Further reading

Liu, J., Hekkenberg, R., Quadvlieng, F., Hopman, H., Zhao, B., 2017. An integrated empirical manoeuvring model for inland vessels. Ocean Eng. 137, 287–308. https://doi.org/10.1016/j.oceaneng.2017.04.008.